AMERICAN SOCIETY FOR MICROBIOLOGY | Journal of Virology®

VIRUS-CELL INTERACTIONS

Catch Me if You Can: the Crosstalk of Zika Virus and the Restriction Factor Tetherin

Marie-Luise Herrlein,[a] Paul Schmanke,[a] Fabian Elgner,[a] Catarina Sabino,[a] Sami Akhras,[a] Daniela Bender,[a] Mirco Glitscher,[a] Denna Tabari,[b] Catharina Scholl,[b] Julia Stingl,[c] Eberhard Hildt[a,d]

[a]Department of Virology, Paul-Ehrlich-Institut, Langen, Germany
[b]Research Division, Federal Institute for Drugs and Medical Devices, Bonn, Germany
[c]Institute of Clinical Pharmacology, University Hospital of RWTH Aachen, Aachen, Germany
[d]German Center for Infection Research (DZIF), Braunschweig, Germany

ABSTRACT Zika virus (ZIKV) is a flavivirus that is mainly transmitted by *Aedes* mosquitos and normally causes mild symptoms. During the outbreak in the Americas in 2015, it was associated with more severe implications, like microcephaly in newborns and the Guillain-Barré syndrome. The lack of specific vaccines and cures strengthens the need for a deeper understanding of the virus life cycle and virus-host interactions. The restriction factor tetherin (THN) is an interferon-inducible cellular protein with broad antiviral properties. It is known to inhibit the release of various enveloped viruses by tethering them to each other and the cell membrane, thereby preventing their further spread. On the other hand, different viruses have developed various escape strategies against THN. Analysis of the cross-talk between ZIKV and THN revealed that, despite a strong induction of THN mRNA expression in ZIKV-infected cells, this is not reflected by an elevated protein level of THN. Contrariwise, the THN protein level is decreased due to a reduced half-life. The increased degradation of THN in ZIKV infected cells involves the endo-lysosomal system but does not depend on the early steps of autophagy. Enrichment of THN by depletion of the ESCRT-0 protein HRS diminishes ZIKV release and spread, which points out the capacity of THN to restrict ZIKV and explains the enhanced THN degradation in infected cells as an effective viral escape strategy.

IMPORTANCE Although tetherin expression is strongly induced by ZIKV infection there is a reduction in the amount of tetherin protein. This is due to enhanced lysosomal degradation. However, if the tetherin level is rescued then the release of ZIKV is impaired. This shows that tetherin is a restriction factor for ZIKV, and the induction of an efficient degradation represents a viral escape strategy. To our knowledge, this is the first study that describes and characterizes tetherin as a restriction factor for the ZIKV life cycle.

KEYWORDS Zika virus, flavivirus, tetherin, BST-2, HRS, ZIKV

Zika virus (ZIKV) has caught international attention due to the epidemics it caused in 2015 in the South Pacific as well as in South and North America. The mosquito-borne flavivirus normally causes only mild, flu-like symptoms like fever and rash. However, it has also been associated with neurological complications like the Guillain-Barré syndrome. During pregnancy, ZIKV infection can lead to congenital malformations like microcephaly of the infant, preterm birth, or fetal loss. Because there is no specific treatment or vaccine available against ZIKV, it is crucial to further understand the virus life cycle and gain more insights into virus-host interactions (1, 2).

ZIKV is a single-stranded, positive-sense RNA virus. The 10.7 kb genome consists of a single open reading frame (ORF), which is flanked by two untranslated regions (UTR).

Editor J.-H. James Ou, University of Southern California

Address correspondence to Eberhard Hildt, Eberhard.Hildt@pei.de.

The authors declare no conflict of interest.

Received 14 December 2021
Accepted 16 December 2021
Accepted manuscript posted online 22 December 2021
Published 23 February 2022

The polyprotein encoded by the ORF is cleaved by virus and host proteases into three structural and seven nonstructural proteins: capsid (C), precursor of membrane/membrane (prM/M), envelope (E), and the nonstructural proteins NS1, NS2A, NS2B, NS3, NS4A, NS4B, and NS5. The mature viral particle comprises the nucleocapsid, formed by the C protein, which encloses the viral RNA and is surrounded by a lipid bilayer, in which the E and M proteins are embedded (3–5).

Transmission of ZIKV mainly occurs via mosquito bites; however, transmission via sexual contact or blood transfusion and vertical transmission from mother to child has also been described (6–10) After transmission, entry into the host cells is mediated by several receptors, like DC-SIGN, TIM-1, and TAM receptors (11). In addition, the role of the epidermal growth factor receptor (EGFR) for ZIKV entry has been suggested recently (12). After uptake of flavivirus particles via clathrin-mediated endocytosis and low pH-dependent fusion of the viral and endosomal membrane, the viral genome is released into the cytosol, where the polyprotein is translated and cotranslationally inserted into the endoplasmic reticulum (ER) for cleavage (13). Reorganization of the ER in infected cells leads to the formation of replication factories, invaginations of the ER membrane that represent the site of viral replication (14). The late stages of the ZIKV life cycle are less resolved. Virion assembly and maturation take place within the reorganized secretory pathway and most likely involve tracts of the trans-Golgi network, which cause a rearrangement of the virus surface and cleavage of the prM by furin (15, 16). ZIKV release is thought to involve vesicle carriers, but their origin is not entirely clear. For exit from the host cell, different mechanisms like a fusion of the vesicle carrier with the host membrane and secretion of vesicles containing single or multiple viral particles are discussed (13, 17, 18).

Tetherin (THN) is an interferon-inducible membrane protein that has been described to restrict the release of various enveloped viruses, like retroviruses (HIV-1), filoviruses (Ebola and Marburg viruses), and herpesviruses (KSHV), among others (19–23). Concerning flaviviruses, THN has been described to inhibit Dengue virus (DENV) release at low multiplicity of infection (MOI) as well as Japanese encephalitis virus (JEV) release (24, 25).

THN comprises an N-terminal cytoplasmic domain followed by a transmembrane helix, an extracellular, glycosylated coiled-coiled domain, and a C-terminal glycosylphosphatidylinositol (GPI) anchor, which allows for a second membrane insertion. With two membrane insertions linked by a molecular spacer, THN can bind budding viruses to the cell membrane and each other and prevent their further spread (20, 26, 27). Besides virus restriction, THN has been stated to act in the same way on exosomes and thereby intervene with their fate (28).

The broad antiviral impact of THN has been controversially discussed probably also because several viruses have evolved successful escape strategies to counteract its restriction (29). Most prominently, the HIV-1 protein Vpu, but several other viral proteins have also been observed to antagonize THN function by inhibiting its anterograde transport or recycling by inducing its degradation or even without removing it from the cell surface (19, 20, 30–32).

In this study, we aimed to characterize the cross-talk between THN and ZIKV. Therefore, the effect of ZIKV on the mRNA expression and protein amount of THN and the impact of THN on the release of ZIKV were studied.

RESULTS

ZIKV infection triggers a strong induction of THN mRNA expression. For identification of deregulated genes in ZIKV infected cells, microarray analyses were performed of RNA isolated 48 h after infection of HaCat cells with either the Polynesia or Uganda strains (Fig. 1A). RNA isolated from uninfected cells served as control. For both ZIKV strains, among other interferon-stimulated genes, a strong induction of the BST-2 gene encoding THN was observed. This was further confirmed by qPCR analysis of RNA isolated from HaCat, HT-1080, and A549 cells at 24 h, 48 h, or 72 h after infection. The qPCR revealed a more than 100-fold induction of BST-2 expression in ZIKV-infected

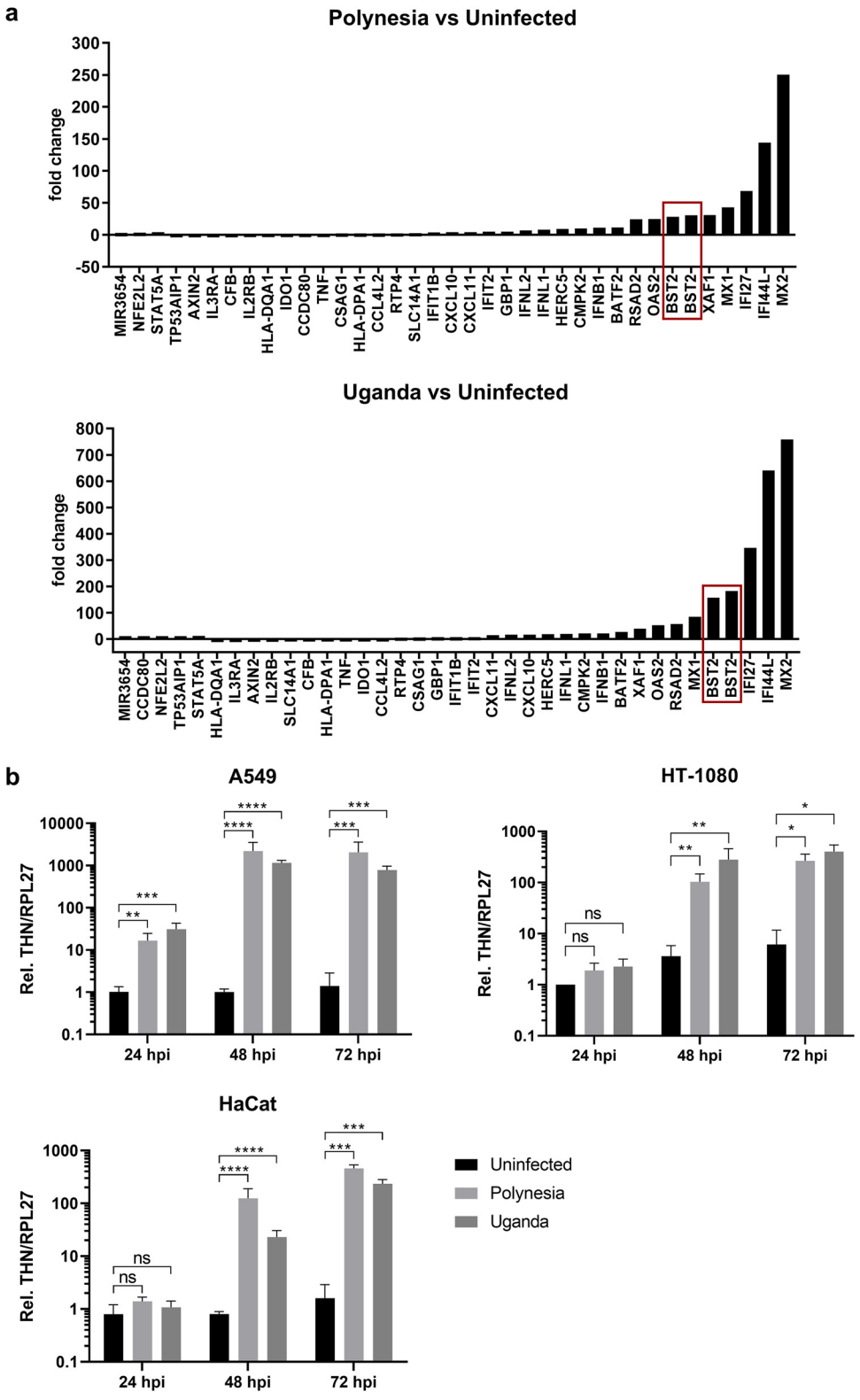

FIG 1 Expression of THN is strongly induced after ZIKV infection. (A) Identification of deregulated genes in ZIKV-infected HaCat cells 48 h pi by microarray analysis, referred to as the uninfected control. Infection with both ZIKV strains resulted in a strong upregulation of BST2 (verified by two different spots on the array), which encodes THN (n = 1). (B) Quantification of THN mRNA levels in A549, HaCat, and HT-1080 cells by qPCR at 24, 48, and 72 h pi at a MOI of 0.1. All values were normalized to the uninfected control at the 24 h time point. More than 100-fold induction of THN mRNA expression could be seen in infected versus uninfected HaCat and HT-1080 cells and more than 1000-fold induction in infected compared to uninfected A549 cells.

HaCat and HT-1080 cells and more than 1000-fold induction in ZIKV-infected A459 cells (Fig. 1B). These data indicate that both ZIKV strains triggered strong induction of BST-2 expression.

Increased expression of BST-2 in ZIKV infected cells fails to correlate with an elevated protein amount of THN. To study whether the strong induction of BST-2 expression in ZIKV-infected cells is reflected by an elevated protein level of THN, Western blots of the cellular lysates derived from ZIKV (Polynesia or Uganda)-infected cells were performed (Fig. 2A). In uninfected A549 cells, the endogenous level of THN is low. Despite the strong induction of BST-2 expression in ZIKV-infected cells, there was no THN detectable also after infection. THN-overexpressing Vero cells (Vero-THN) served as a positive-control. This contrasts with HEV-infection, which has been described before to induce THN protein levels in Huh7 cells (33) and causes an upregulation of THN in a detectable range as well in A549/D3 cells (Fig. 2B). To further characterize the impact of ZIKV infection on the amount of THN, THN-overexpressing cells were infected with ZIKV (Fig. 2C). Surprisingly, the blot shows a significant decrease in the amount of THN in ZIKV-infected compared to uninfected cells. The decreased amount of THN in ZIKV-infected cells was further confirmed by confocal immunofluorescence microscopy of ZIKV infected Vero-THN cells using THN- and ZIKV E protein-specific antibodies (Fig. 2D). In accordance with the Western blot, quantification of the corrected total cell fluorescence (CTCF) revealed a significantly reduced amount of THN in ZIKV infected cells compared to the control (Fig. 2E). In addition to the generally reduced signal intensity, the membrane localization of THN was no longer detectable.

To clarify whether the reduction of overproduced THN was caused by ZIKV or was nonspecifically due to cellular innate immune response pathways, HT-1080-THN cells were subjected to poly(I·C) treatment for 16 h or 24 h (Fig. 2E). No reduction but a slight increase of THN amount was observed in poly(I·C) treated cells, which might be caused by an upregulation of endogenous THN due to interferon (IFN) stimulation. This increase, however, was not significant.

Taken together, these data show that the strong induction of BST-2 expression was not reflected by an elevated amount of THN protein in ZIKV infected cells. In contrast, a significantly decreased protein level of THN was found in ZIKV-infected, THN-overproducing cells.

Decreased half-life of THN in ZIKV-infected cells. To further characterize the obvious lack of correlation between increased mRNA expression and decreased protein amount of THN, the half-life of THN in ZIKV-infected cells was analyzed (Fig. 3). For this purpose, translation was blocked by the presence of 71 μM CHX in ZIKV (Uganda strain)-infected and uninfected cells, and the amount of THN was determined at several time points by Western blotting. For the uninfected cells, nonlinear regression revealed a half-life of THN of 526 min. In infected cells, the half-life was strongly reduced (141 min) compared to uninfected cells. This indicated an increased degradation of THN protein in ZIKV-infected cells.

Inhibition of lysosomal protein degradation partly restores THN protein levels in ZIKV infected cells. To analyze in more detail the increased degradation of THN, ZIKV Uganda-infected cells were treated with various inhibitors of cellular protein degradation pathways for 8 h. The impact of these inhibitors on the amount of THN was analyzed by Western blotting using THN- and ZIKV-E-specific antibodies (Fig. 4A). While inhibition of proteasomal protein degradation by Bortezomib and MG132 did not affect or further decrease the THN signal, inhibition of lysosomal protein degradation by NH_4Cl, chloroquine, and BFLA resulted in an increase of the THN signal in the infected cells. However, inhibition of early steps of autophagy by the PI3K-Inhibitor LY294002 did not affect the amount of THN.

This was reflected by immunofluorescence microscopy of Vero-THN cells 24 h after infection with ZIKV Polynesia or Uganda at a MOI of 5. Cells were analyzed for THN and either the lysosomal marker LAMP2 or autophagosomal LC3 (Fig. 4B). While there was colocalization of the remaining intracellular THN signal with LAMP2 in the infected cells, LC3 was only found adjacent, but not colocalizing with THN. Moreover, inhibition

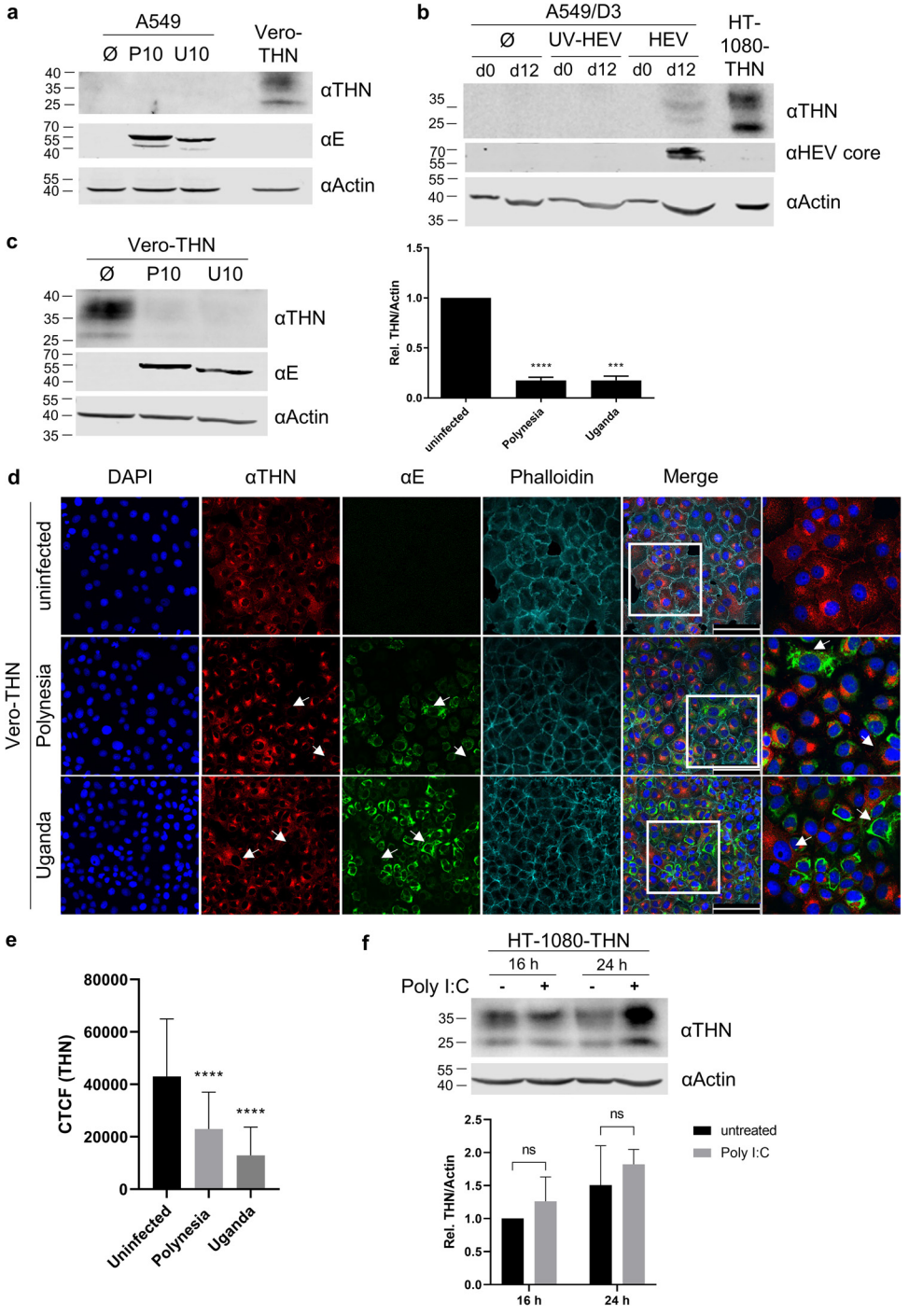

FIG 2 ZIKV infection leads to a reduced amount of THN. (A) Western blot analysis of A549 cells at 24 h pi at a MOI of 10 with ZIKV Polynesia or Uganda. Vero-THN cells served as control. Despite elevated BST-2 expression, THN protein is not detectable after ZIKV infection in A549 cells. (B) Western blot analysis of A549/D3 cells at 0 and 12 days after infection with HEV. UV-inactivated HEV and HT-1080-THN cells served as negative- and positive-controls, respectively. In contrast to ZIKV, HEV infection results in elevated amounts of THN that are detectable by Western blotting. (C) Western blot of Vero-THN cells at 24 h pi at a MOI of 10. ZIKV infection strongly decreased THN protein levels. (D) Immunofluorescence microscopy of Vero-THN cells left uninfected or after infection with ZIKV Polynesia or Uganda 24 h pi at a MOI of 0.1. THN and ZIKV E were visualized with specific antibodies in red and green, respectively. Nuclei were stained with DAPI (blue) and the actin cytoskeleton with phalloidin-Atto633 (cyan). Scale bars indicate 100 μM. Expanded fields of view are shown without the actin signal to ease comparison. A strong reduction of THN signal in infected compared to uninfected cells was observed, as indicated by the arrows. (E) The total fluorescence per cell of cells depicted in (D) was calculated using the software Fiji with the formula corrected total cell fluorescence

(Continued on next page)

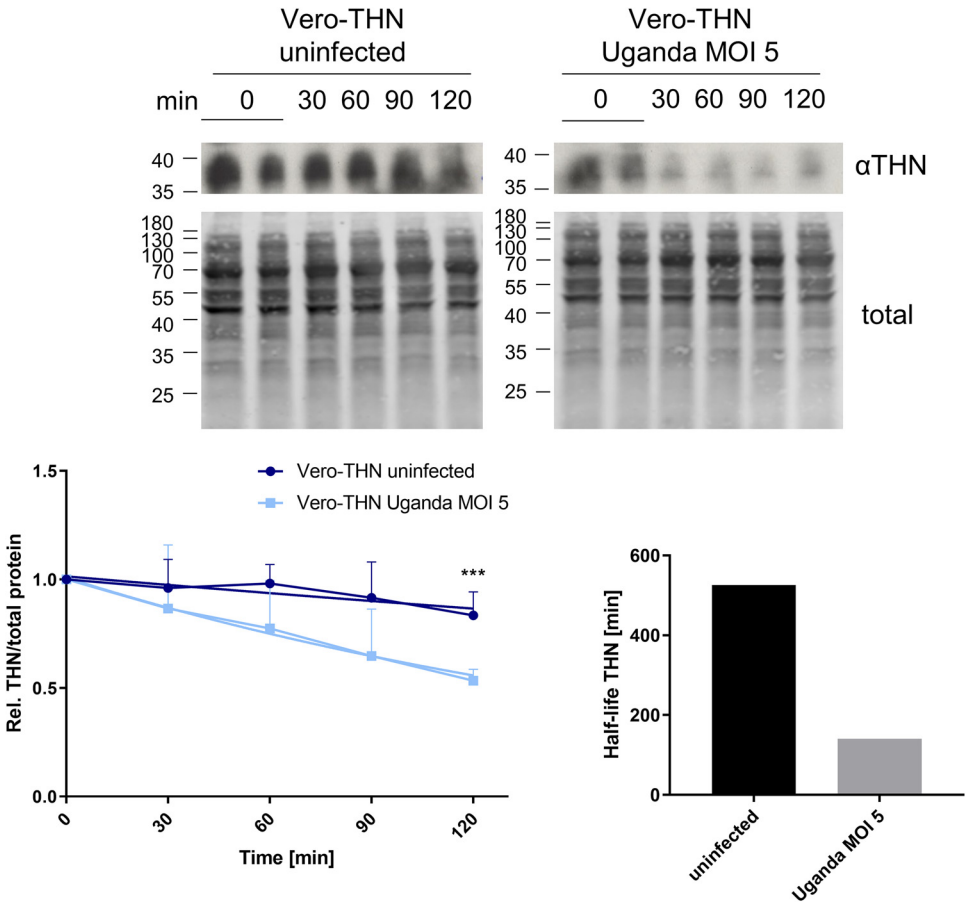

FIG 3 ZIKV infection causes a reduced THN half-life. Vero-THN cells were treated with CHX 16 h pi and analyzed by Western blotting at the indicated time points. All values were normalized to the onset of the treatment. Half-lives were calculated by a nonlinear regression equation based on the mean values of at least five independent experiments and are shown in the bottom right graph. THN protein half-life is significantly shorter in infected cells, indicating an elevated degradation of THN compared to uninfected cells.

of lysosomal acidification by BFLA leads to an accumulation of THN and LC3 in LAMP2-positive structures.

Altogether, these data point toward a lysosomal degradation of THN in ZIKV infected cells, which does not require early steps of autophagy.

ZIKV release is not impaired in THN-overexpressing cells. The data described above indicate that ZIKV strongly affects the amount of THN, suggesting that this could be a strategy to escape from THN-dependent restriction. To experimentally investigate the potential impact of THN on ZIKV release, Vero-THN cells or cells stably transfected with an empty vector control (Vero eV) were infected with ZIKV Polynesia or Uganda at different MOIs. Supernatants were harvested at 16 h postinfection (pi) and the number of viral particles was determined by plaque assays (Fig. 5A). No impact of the THN-overexpression on the amount of released infectious viral particles was observed. Comparable results were obtained for stably THN-overproducing HT-1080 cells (HT1080-THN). Compared to the HT-1080 control cells, no significant difference in the amount of released viral particles was observed. This was also confirmed by qPCR analyses, which revealed no difference in the amount of released extracellular viral

FIG 2 Legend (Continued)
($CTCF_{THN}$) = integrated $density_{THN}$ (area of selected cell × mean fluorescence of background readings). Per condition, a minimum of 67 cells was measured. In the case of infected cells, cells with a $CTCF_{ZIKV\ E} \geq 8000$ were considered. (F) Western blot of HT-1080-THN cells 16 h and 24 h after Poly I:C treatment. A slight but not significant increase of THN amount was observed in Poly I:C-treated cells.

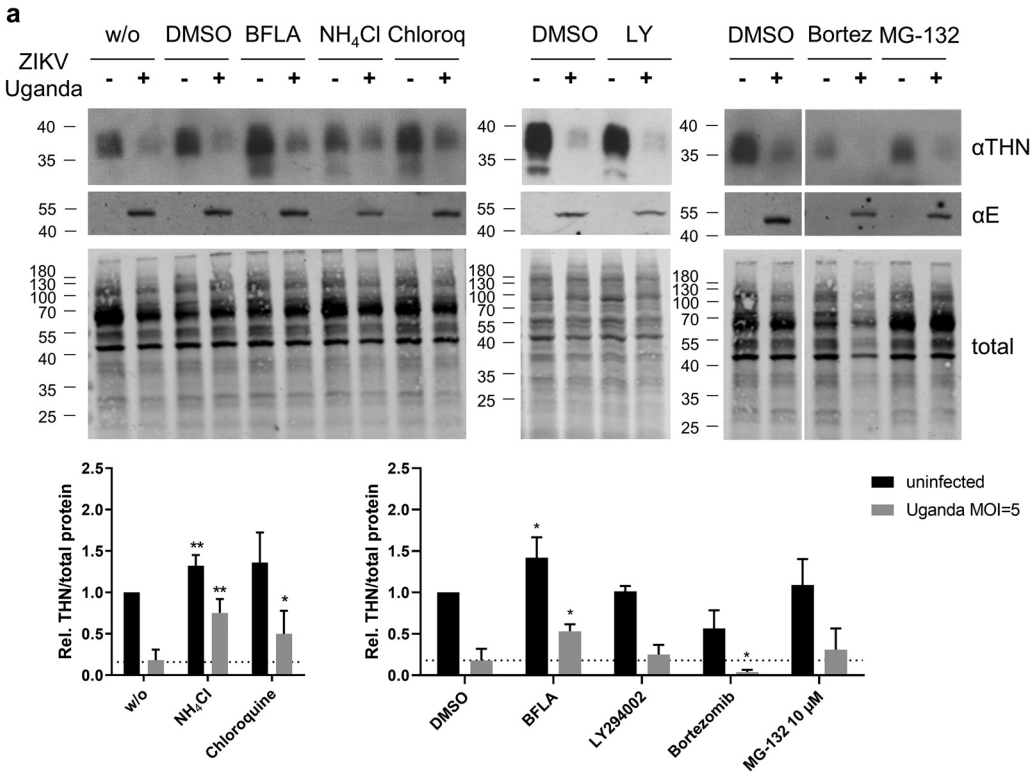

FIG 4 Lysosomal protein degradation is responsible for reduced THN levels in ZIKV infected cells. (A) THN-overexpressing Vero cells were treated with inhibitors of different protein degradation pathways after infection with ZIKV Uganda and THN levels were analyzed by Western blotting. Values were normalized to the uninfected untreated (w/o) or DMSO control, depending on the solvent of the respective inhibitor. Inhibition of lysosomal acidification partly restored THN levels, while inhibition of early steps of autophagy or proteasomal degradation did not change or even further decreased the THN signal. (B) Immunofluorescence microscopy of uninfected or ZIKV Polynesia/Uganda infected cells 24 h pi at a MOI of 5. At this time point and MOI, all of the cells are typically infected. On the left side, THN (green) and the lysosomal marker LAMP-2 (red), on the right side, THN (red) and the autophagosomal marker LC3 (green) were stained with specific antibodies. Nuclei were visualized with DAPI (blue). Scale bars indicate 30 μM. In untreated cells, the remaining intracellular amount of THN is colocalizing with the LAMP-2, but not with LC3. BFLA treatment results in the accumulation of THN within lysosomal structures.

genomes between THN-overproducing and control cells in both cell lines (Fig. 5B). At the first glance, this suggests that THN fails to restrict ZIKV release. However, as described above (Fig. 2B), Western blotting of cellular lysates derived from uninfected or ZIKV-infected cells revealed for both viral strains a strong reduction in the amount of THN compared to the uninfected control. This showed that even overproduced THN was efficiently degraded in ZIKV infected cells, and, hence, ZIKV could escape from its restricting function.

Knockdown of ESCRT-0 protein HRS results in strongly increased THN protein levels. Considering the rapid turnover even of overproduced THN in ZIKV-infected cells, it was attempted to prevent the sorting of THN into lysosomes. In previous studies, the ESCRT-0 protein HRS (also called HGS) has been identified as a key factor for THN degradation in HIV-infected cells. (34) To examine this role of HRS in the context of ZIKV infection, HT-1080-THN cells or the wild-type control were treated with HRS siRNA for 48 h before infection with ZIKV Polynesia or Uganda at a MOI of 0.1 or 5. Cells were harvested at 24 h pi and the lysates were analyzed for HRS and THN protein levels by Western blotting (Fig. 6).

The efficient knockdown of HRS indeed led to a strong increase of the THN signal in uninfected HT-1080-THN cells and after infection at low MOI. At a MOI of 5, the THN signal after HRS knockdown still exceeded the level in the control siRNA-transfected cells. However, a decrease of THN compared to the uninfected cells remained.

Taken together, these data indicate that silencing of HRS is an efficient tool to increase the THN level in ZIKV infected cells.

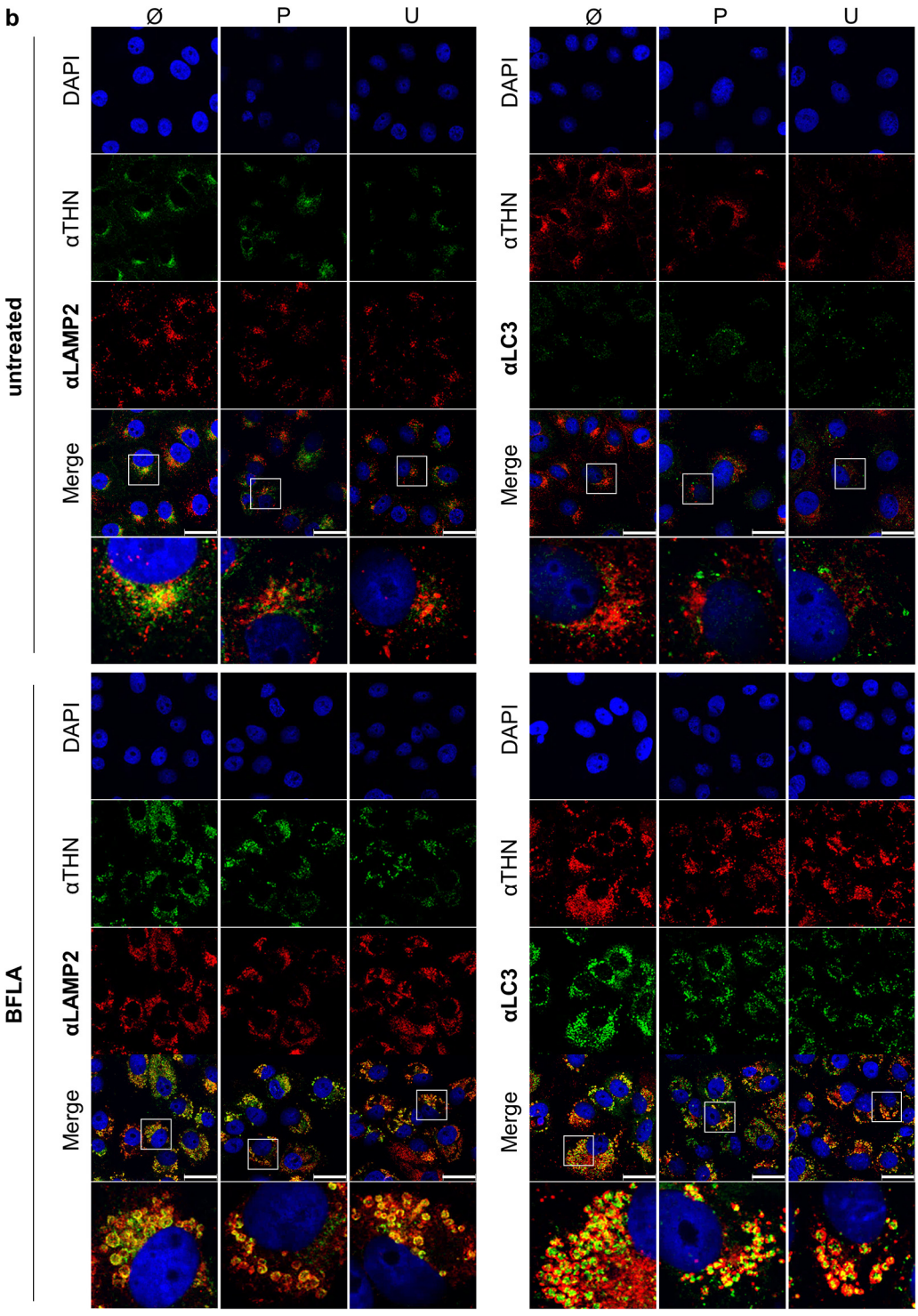

FIG 4 (Continued)

Increased THN level reduces ZIKV release. To clarify, if the elevation of THN protein level in ZIKV-infected cells leads to an impaired release of ZIKV, extracellular viral titers of wild type and THN-overexpressing HT-1080 cells were compared either after HRS knockdown or after transfection with a control siRNA (Fig. 7A). In the control siRNA-transfected cells, no difference in the amount of extracellular viral particles could be observed between the two cells lines. However, after the specific knockdown of

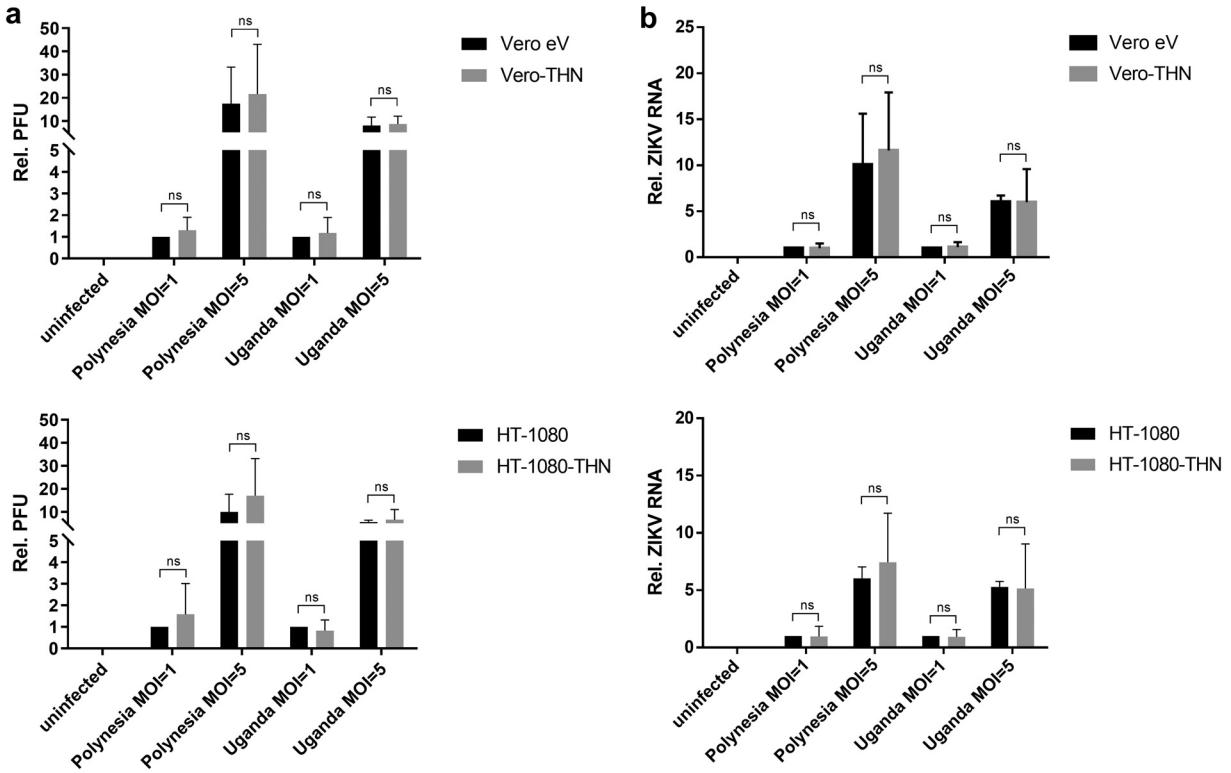

FIG 5 ZIKV escapes THN restriction. Vero or HT-1080 cells stably overexpressing THN (Vero-THN/HT-1080-THN) and the respective empty vector or wild-type control (Vero eV/HT-1080) were infected at a MOI of 1 or 5. (A) The amount of released infectious viral particles was determined by plaque assay. (B) Extracellular viral genomes were analyzed by qPCR. Relative values referred to the empty vector/wild-type control infected at a MOI of 1 with the respective ZIKV strain. No impact on THN-overexpression on the amount of released virus and viral genomes was observed.

HRS, significantly lower viral titers were detected in the supernatant of THN-overexpressing cells compared to wild-type cells.

To understand if the lower extracellular viral titers in HT-1080-THN cells are caused by a reduced release or reflect an increased attachment of the remaining ZIKV input, a binding assay was performed (Fig. 7B). HT-1080 and HT-1080-THN cells were transfected either with HRS or control siRNA 48 h after transfection. Cells were prechilled for 30 min before they were infected with ZIKV Polynesia or Uganda at a MOI of 0.1 for 1 h at 4°C. The bound viral genomes were then quantified by qPCR. No significant difference in the amount of bound virus between wild type and THN-overexpressing HT-1080 cells was observed. This implied that the reduced extracellular ZIKV titers in HT-1080-THN cells after HRS knockdown were not due to increased binding of virus input to the cells but resulted from a reduction of ZIKV release.

THN impairs ZIKV spread after knockdown of HRS. The impact of THN on ZIKV release was further elucidated by immunofluorescence microscopy. HT-1080 and HT-1080-THN cells were transfected with HRS or control siRNA and infected 48 h later with ZIKV Polynesia or Uganda at a MOI of 0.1. Cells were fixed 24 h pi and stained with THN- and ZIKV E-specific antibodies (Fig. 8). After HRS knockdown, the number of ZIKV-infected cells was reduced in THN-overexpressing compared to wild-type cells. This was observed both for the Polynesia and Uganda ZIKV strains and indicates a reduced virus spread due to the increased THN protein level.

The knockdown of HRS also led to reduced cell proliferation, as described before. (35) At the time point of infection (48 h posttransfection), HRS and control siRNA-transfected cells, therefore, varied in cell number and density, which might lead to a different susceptibility, and were not directly comparable. Yet, when comparing control siRNA-transfected HT-1080 and HT-1080-THN cells, no difference in the number of

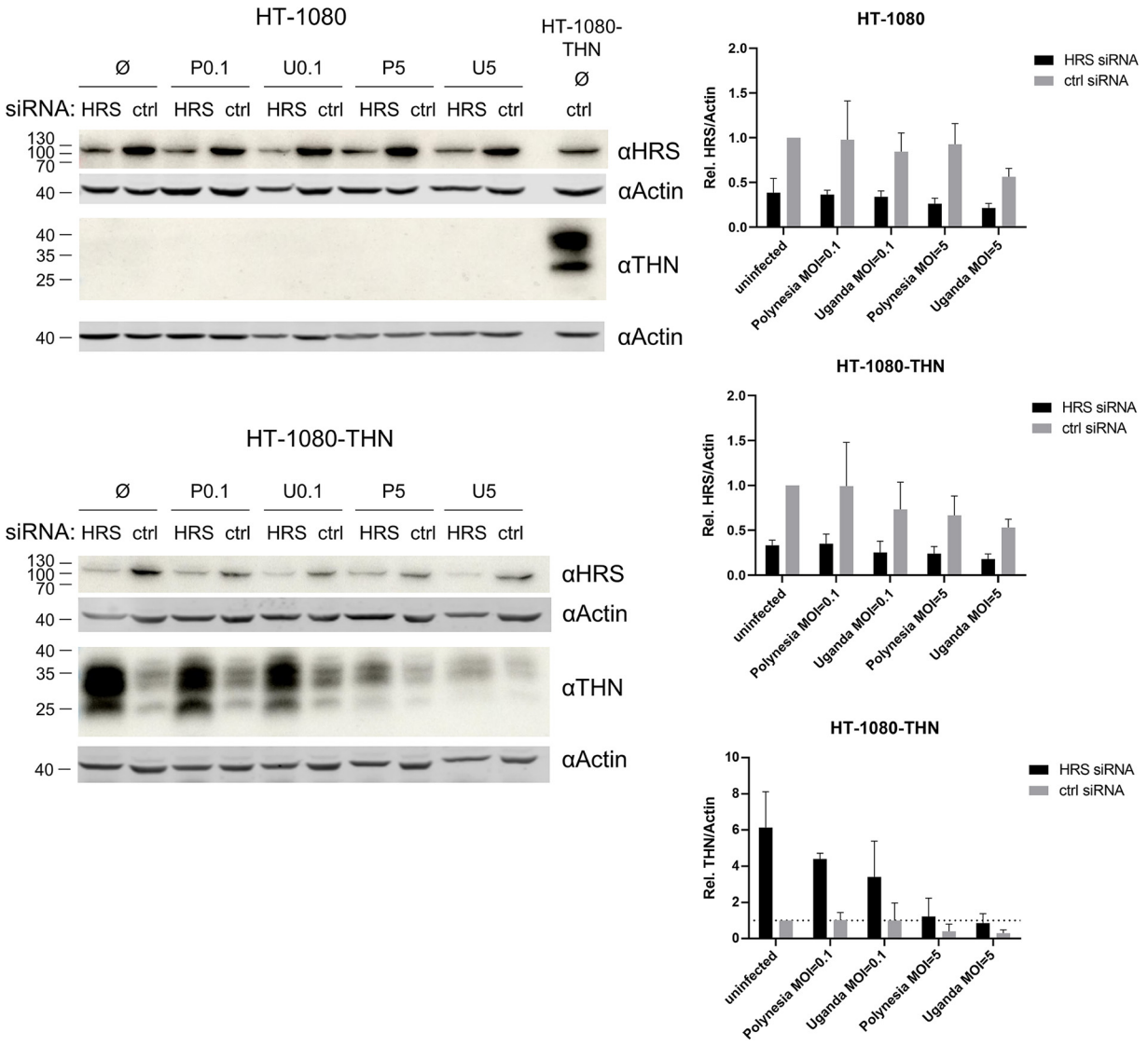

FIG 6 Knockdown of HRS with siRNA results in THN accumulation. THN-overexpressing and wild-type HT-1080 cells were transfected with HRS or control siRNA and infected 48 h later at a MOI of 0.1 or 5. Cells were analyzed by Western blotting 24 h pi for HRS and THN. For HT-1080 cells, one lane with HT-1080-THN cells served as positive-control in terms of THN detection. Quantification of HRS and THN protein amounts were normalized to the uninfected, control siRNA-transfected cells. THN accumulated in HT-1080-THN cells after HRS knockdown compared to control siRNA-transfected cells. However, a decrease of THN signal after infection at high MOI compared to the uninfected cells was still observed.

ZIKV-infected cells, and, hence, viral spread was visible. This indicates that the knockdown of HRS was necessary for the observed reduction of viral spread in THN-overexpressing cells.

Imaging with a higher resolution of HT-1080-THN cells after HRS knockdown enabled a closer look at the interaction between THN and ZIKV (Fig. 9). The main proportion of the ZIKV E protein was localized in the perinuclear region and did not colocalize with the THN signal. However, a smaller fraction of E was present in more peripheral structures. For this fraction, a colocalization with THN was observed both in ZIKV Polynesia and Uganda infected cells.

Taken together, this indicates the trapping of ZIKV in THN-positive structures after the knockdown of HRS, which results in a reduction of virus spread.

To exclude possible off-target effects of the used HRS siRNA, the quantification of the THN amount, extracellular viral titers, and proportion of ZIKV-positive cells as well

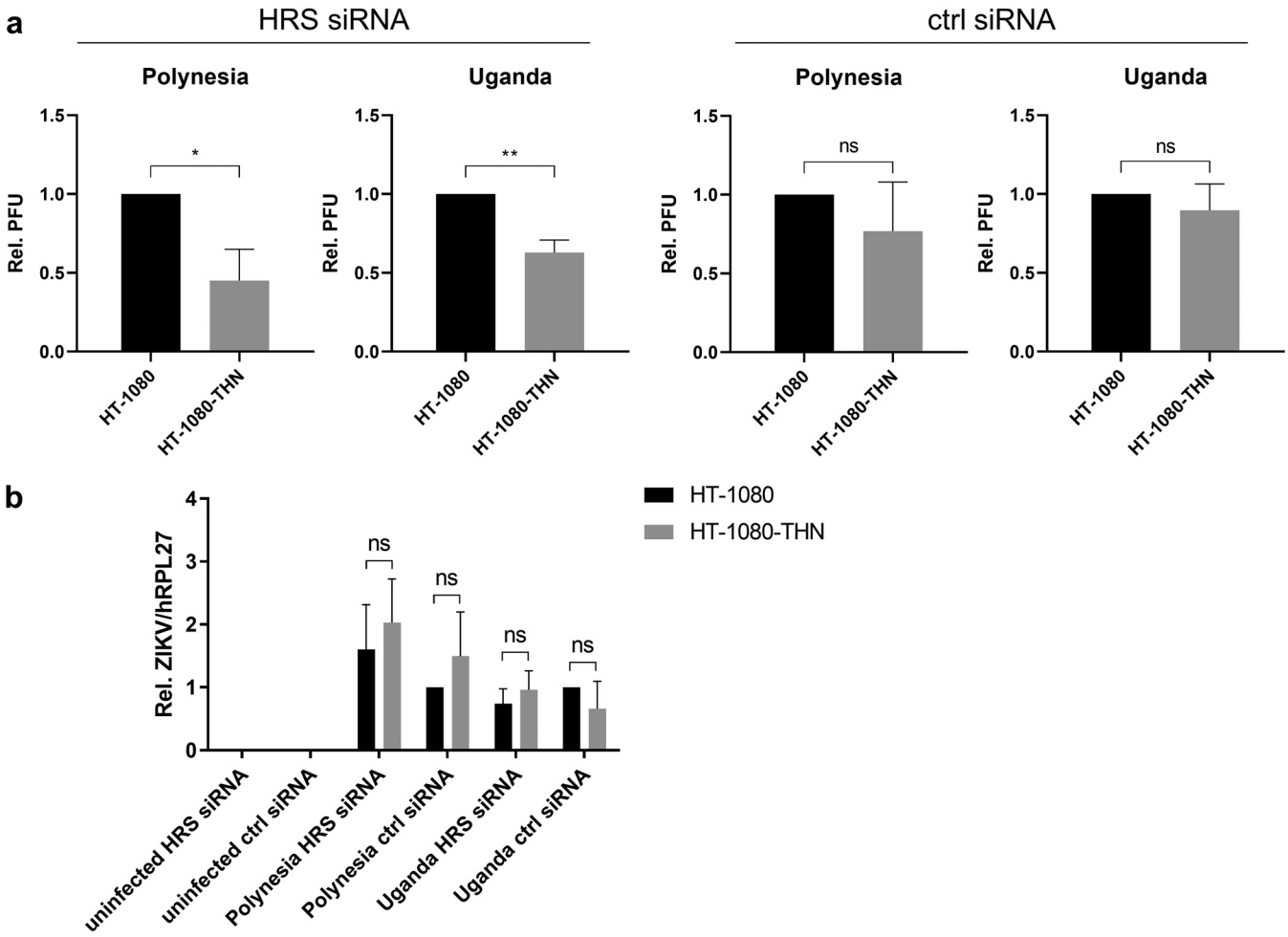

FIG 7 Reduction of ZIKV release from THN-overexpressing cells after HRS knockdown. (A) Extracellular viral titers from HT-1080 and HT-1080-THN cells transfected with either HRS or control siRNA were determined by plaque assay 24 h pi at a MOI of 0.1. Values were normalized to the HRS or control siRNA-transfected wild-type cells. While no significant difference between HT-1080 and HT-1080-THN extracellular viral titers was observed after transfection of control siRNA, titers of HRS siRNA-transfected HT-1080-THN cells were lower than HT-1080 cells. (B) ZIKV binding assay. HT-1080 and HT-1080-THN cells transfected either with HRS or control siRNA were prechilled 30 min and then infected 1 h at 4°C. Bound viral genomes were determined by qPCR. Values were normalized to control siRNA-transfected HT-1080 cells. No significant difference in ZIKV binding was observed, neither in HRS nor in control siRNA-transfected cells.

as the analysis of THN-ZIKV E colocalization was repeated after transfection with a second HRS siRNA and infection with ZIKV Polynesia (Fig. 10). The obtained data confirmed the reduction of ZIKV release and spread due to THN accumulation in THN-overexpressing cells after HRS knockdown.

DISCUSSION

The restriction factor THN is known to impair the release and spread of various enveloped viruses (19). In the case of flaviviruses, there are so far two reports describing an inhibitory effect of THN on the release of DENV and JEV (24, 25). In our study, microarray analysis and qPCR revealed a strong induction of BST-2 expression in ZIKV-infected HaCat, HT-1080, and A549 cells. In addition, an increased expression of BST-2 has been previously observed in ZIKV-infected human neural stem cells (lt-NES) (36). This gave rise to further characterization of the mutual interaction of THN and ZIKV in this study.

Surprisingly, the induction of BST-2 expression was not reflected by an elevated protein amount of THN. On the contrary, the THN signal in THN-overexpressing cells was heavily reduced upon ZIKV infection. Vice versa, no effect of THN-overexpression on ZIKV release could be seen. Hence, the efficient degradation of THN in ZIKV

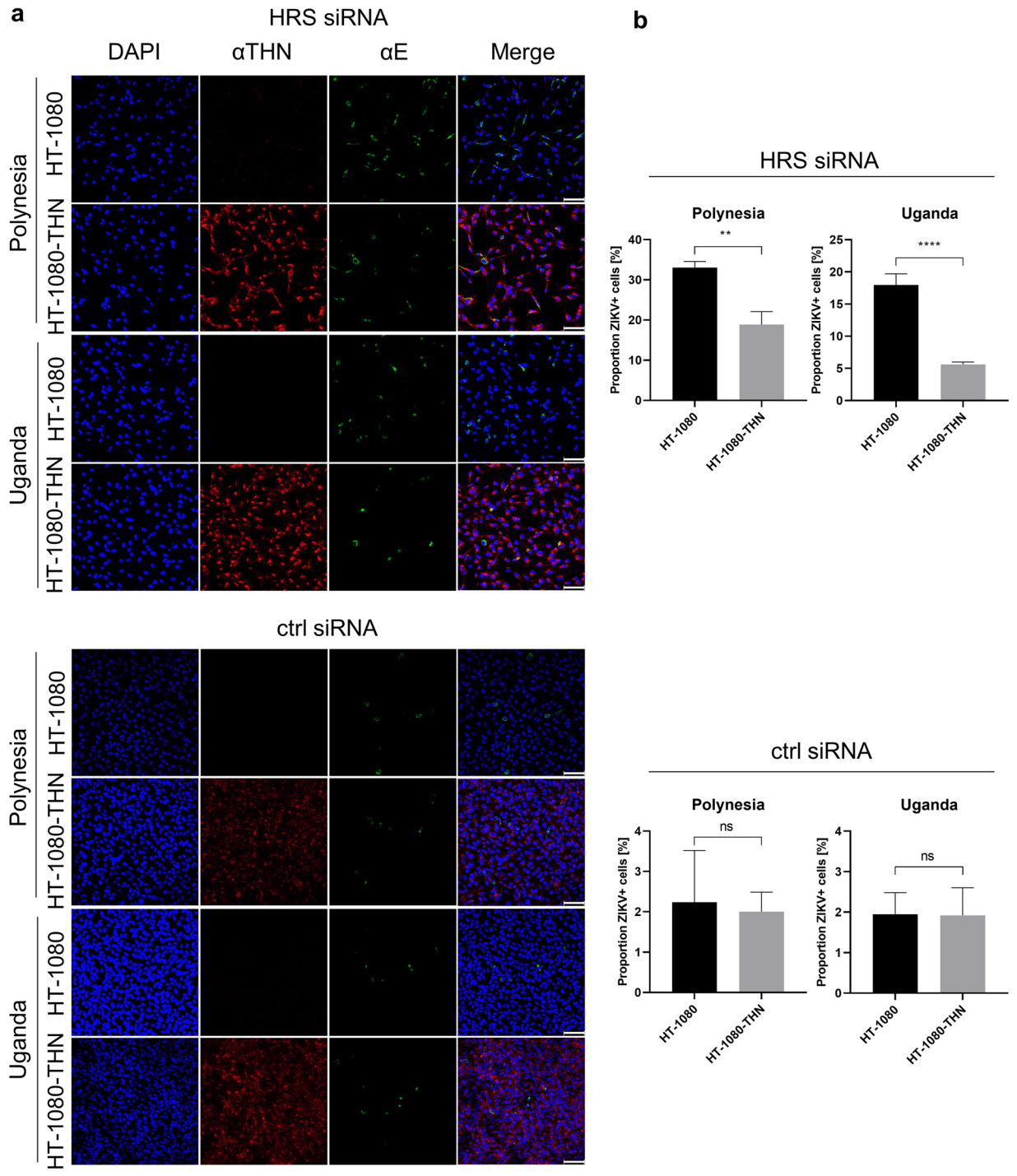

FIG 8 Reduced ZIKV spread in HT-1080-THN cells after HRS knockdown. (A) Immunofluorescence microscopy of HT-1080 and HT-1080-THN cells transfected either with HRS or control siRNA and infected with ZIKV Polynesia or Uganda for 24 h at a MOI of 0.1. THN and ZIKV E were visualized with specific antibodies in red and green, respectively; nuclei were stained with DAPI (blue). Scale bars indicate 100 μM. (B) Quantification of ZIKV-positive cells in three fields of view of cells depicted in (A). After transfection with HRS siRNA, the number of infected cells was lower for HT-1080-THN compared to HT-1080 cells. This was not the case in control siRNA-transfected cells. Due to reduced proliferation and lower cell density after HRS siRNA transfection, a direct comparison between HRS and control siRNA-transfected cells was not possible.

replicating cells prevents an inhibitory effect of THN overexpression on ZIKV release. In light of this, it can be assumed that the enhanced degradation of THN protein in ZIKV infected cells represents an effective escape mechanism to prevent the restriction of virus release by THN.

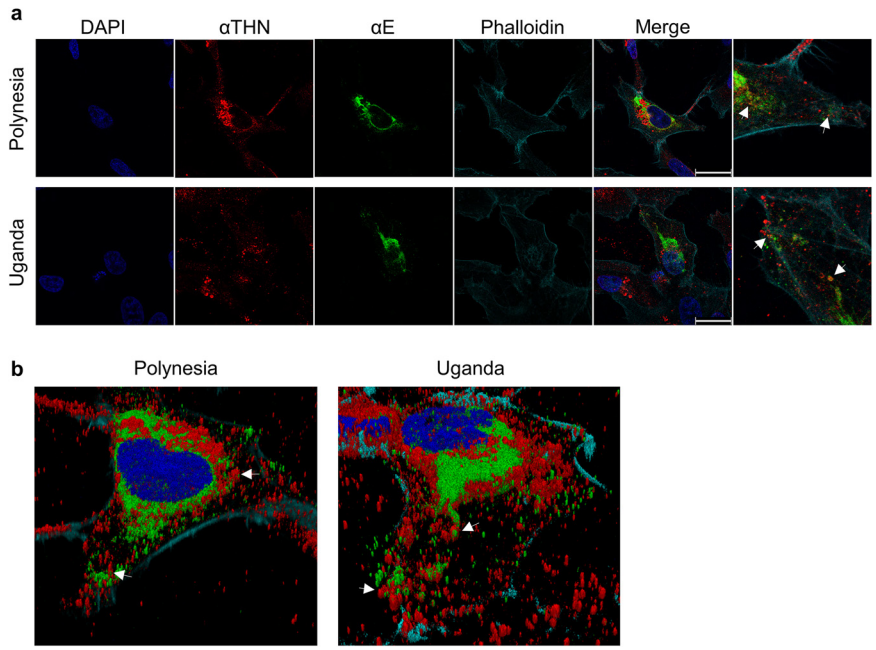

FIG 9 ZIKV E partly colocalizes with THN in HT-1080-THN cells after HRS knockdown. (A) Images with higher magnification (100× objective) of HRS siRNA-transfected HT-1080-THN cells 24h after infection with ZIKV Polynesia/Uganda at a MOI of 0.1. THN and ZIKV E were visualized with specific antibodies in red and green, respectively; nuclei were stained with DAPI (blue) and the actin skeleton with phalloidin-Atto633. Scale bars indicate 30 μM. A colocalization of ZIKV E and THN was observed in peripheral structures as indicated by the arrows. (B) 3D reconstruction of cells depicted in (A).

ZIKV is known to enhance autophagy and subsequent lysosomal protein degradation. The ZIKV-dependent inhibition of the Akt-mTOR signaling pathway contributes to increased autophagosome formation (37, 38). Interestingly, our data imply no importance of these early steps of autophagy for the enhanced degradation of THN in ZIKV infected cells as inhibitors affecting these early steps had no impact on the THN level in ZIKV infected cells. However, inhibition of lysosomal acidification led to a restoration of THN protein levels. Indeed, under these conditions, an inhibitory effect on the release of ZIKV could be observed (data not shown). Although the amount of E was not affected under these conditions and viral replication was not impaired, it cannot be excluded that the inhibitory effect on the release under these conditions depends on further factors.

Therefore, we aimed to specifically restore the THN protein level in ZIKV infected cells and to investigate the impact on ZIKV release. In HIV-infected cells, HRS is an essential factor for the degradation of THN (34). In light of this, it was investigated whether silencing of HRS expression could be a strategy to specifically rescue the amount of THN in ZIKV infected cells.

Indeed, a strong increase of THN levels after knockdown of HRS in uninfected and ZIKV infected THN-overexpressing cells at a low MOI was observed. In HT-1080 wild-type cells, THN levels were still undetectable after HRS knockdown, which can be explained by the fact that upregulation of THN mRNA expression is not significant in HT-1080 cells at this time point during infection (24 h pi). At a higher MOI, the THN protein signal was still decreased compared to uninfected cells even after HRS knockdown in HT-1080-THN cells. Thus, degradation of THN must be possible via an additional, HRS-independent pathway in ZIKV infected cells. Other proteins like TOM and GGA have been described to act similarly and probably complement or replace ESCRT-0 proteins, which might be one possible way for enhanced THN degradation despite HRS knockdown (39–41). Yet, our data reveal a rescue of THN function after HRS knockdown at low MOI. Under these conditions, an impaired release and spread of ZIKV can be observed in THN-overexpressing compared to the wild-type control cells. Strikingly,

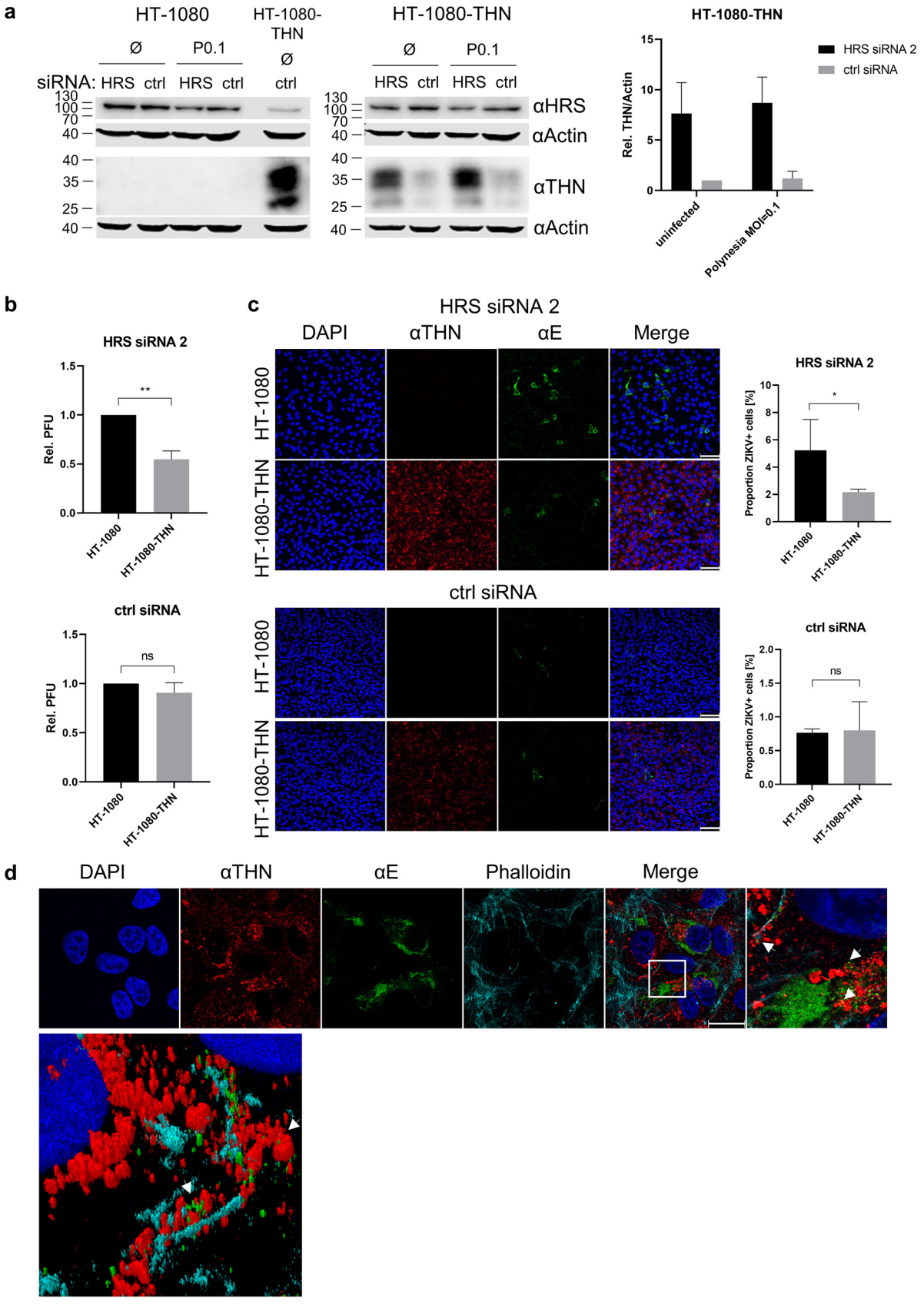

FIG 10 Second HRS siRNA confirms a reduction of ZIKV release and spread in HT-1080-THN cells after HRS knockdown. HT-1080 and HT-1080-THN cells were transfected with HRS siRNA 2 or control siRNA and infected with ZIKV Polynesia at a MOI of 0.1 for 24 h. (A) Cells

(Continued on next page)

no significant effect on the binding of ZIKV was observed at this point. It can therefore be assumed that THN has no impact on free, extracellular viral particles, and its trapping function is restricted to budding virions.

HRS as a part of the ESCRT-0 complex is described to bind ubiquitinated cargo in the endosomal membrane and then recruit further ESCRT-complexes to allow for invagination of the endosomal membrane and multivesicular body (MVB) formation (39, 42). Furthermore, this process is involved in viral budding and the release of several enveloped viruses, including HIV, HBV, and HCV (43–45). Details on the ZIKV release and the involved structures are to this date mostly unknown. However, a role of the endo-lysosomal compartment has been suggested before, due to a reduction of ZIKV release after BFLA treatment (46). Here, we observed an intracellular colocalization of ZIKV E protein with THN, after it was trapped in early endosomes due to HRS depletion. It is assumed that ZIKV particles already interact with THN in endosomes or MVBs and not only on the plasma membrane, which is similar to that described for HBV (47). A general role of these compartments for ZIKV release can therefore be hypothesized but needs to be further validated.

Targets for antiviral treatment that affect multiple viruses are of great importance, especially with regard to new emerging viruses in times of globalization and global warming, the latter leading to the facilitated spread of vector-borne viruses, like arboviruses. In turn, this points out the benefit of host-related over viral targets. In this context, inhibitors of fibroblast growth factors (FGFs) have been recently suggested as antiviral compounds, as FGFs impair the interferon response and were therefore found to promote virus infection (48). Our findings, however, emphasize the discrepancy between enhanced interferon-stimulated gene (ISG) expression and functionality, due to viral escape strategies. The promotion of ISG expression should therefore go along with inhibition of the degradation of interferon-induced proteins, highlighting HRS as a potential antiviral target.

In conclusion, we observed in this study an induced mRNA expression, but enhanced lysosomal protein degradation of THN in ZIKV infected cells, reflecting an effective escape strategy. Prevention of THN degradation by HRS depletion led to a restriction of ZIKV release by THN, which verifies the role of THN for the control of ZIKV release and points out HRS as a potential antiviral target.

MATERIALS AND METHODS

Cell culture and infection. HaCat, A549, Vero, HT-1080, and A549/D3 cells (a subclone of A549 cells, selected for high hepatitis E virus (HEV) susceptibility (49)) were cultivated in DMEM (BioWest, Nuaillé, France), supplemented with 10% FCS (Bio & Sell GmbH, Feucht, Germany), 2 mM L-glutamine (Bio & Sell GmbH, Feucht, Germany) and, respectively, 100 μg/mL penicillin and streptomycin (Paul-Ehrlich-Institut, Langen, Germany) (DMEM complete). Vero cells stably transfected with HA-tagged THN and HT-1080 cells were stably transfected with untagged THN. The respective empty vector and wild-type control were kindly provided by Barbara Schnierle from the Paul-Ehrlich-Institut. Cells were incubated at 37°C with 5% CO_2 and 95% humidity and passaged by trypsinization three times a week.

The ZIKV strains French Polynesia H/PF/2013 and Uganda 976, referred to as "Polynesia" and "Uganda", were used. Both strains were provided by the European Virus Archive goes Global (EVAg). HEV infection and UV inactivation were performed as described by Glitscher et al. (50).

Microarray analysis. Total RNA was extracted from uninfected and ZIKV infected HaCat cells 48 h pi using the miRNeasy minikit (Qiagen, Hilden, Germany), and the gene expression was analyzed as previously described (36).

RNA isolation and qPCR. Cells were harvested with peqGOLD TriFast reagent (PEQLAB Biotechnologie GmbH, Erlangen, Germany) or RNA-solv reagent (Omega Bio-Tek, Norcross, USA) and total RNA was extracted with Chloroform as instructed by the manufacturers. Five micrograms of the isolated RNA were processed for RQ1 DNase I digestion (Promega, Madison, USA) and cDNA synthesis with

FIG 10 Legend (Continued)
were analyzed by Western blotting for HRS and THN. (B) Extracellular viral titers were determined by plaque assay. (C) The number of ZIKV-positive cells was analyzed by immunofluorescence microscopy. THN and ZIKV E were visualized with specific antibodies in red and green, respectively; nuclei were stained with DAPI (blue). Scale bars indicate 100 μM. ZIKV-positive cells were quantified in three fields of view. (D) HT-1080-THN cells transfected with HRS siRNA 2 and infected with ZIKV Polynesia were imaged with higher magnification (100× objective). THN, ZIKV E, and nuclei were visualized as described in (C), the actin skeleton with phalloidin-Atto633. Scale bars indicate 30 μM. The lower panel shows a 3D reconstruction of a section of the cells depicted above.

RevertAid H Minus Reverse Transcriptase (Thermo Fisher, Waltham, USA). Subsequent qPCR analysis was performed in a LightCycler480 device (Roche, Basel, Switzerland) using the Maxima SYBR Green qPCR Master Mix (Thermo Fisher, Waltham, USA) and the following primers: THN (fw): acctgcaaccacactgtgatg, THN (rev): caagctcctccactttcttttgtc, ZIKV (fw): agatcccggctgaaacactg, ZIKV (rev): ttgcaaggtccatctgtccc, RPL27 (fw): aaagctgtcatcgtgaagaac, and RPL27 (rev): gctgtcactttgcgggggtag.

For quantification of extracellular viral genomes, viral RNA was isolated from 140 μL of cell supernatant using the QIAamp Viral RNA minikit (Qiagen, Hilden, Germany) and qPCR was performed using the LightMix Modular Zika Virus (Roche, Basel, Switzerland) according to the manufacturer's instructions.

Virus titration. Quantification of viral titers was done by performing a plaque assay. For this purpose, Vero cells were seeded in 6-well plates at a density of 3×10^5 cells per well. To analyze the amount of extracellular infectious virions, supernatants of infected cells were collected and centrifuged for 5 min at 5000 $\times$ *g* to remove cell debris. Serial dilutions (100 μL) of the supernatants were added to one well, respectively. After removing the input after 2 h pi, cells were overlaid with 0.4% SeaPlaque™ agarose (Lonza, Basel, Switzerland) in DMEM complete. After 5 days, cells were fixed with 4% formaldehyde in PBS, and plaques were visualized with 0.1% crystal violet in 20% ethanol. Subsequently, the plaque forming unit (PFU) was quantified.

SDS-PAGE and Western blot. Cell lysates were generated with radioimmunoprecipitation assay (RIPA) buffer and sonicated for 10 s with 20% power. Equal protein amounts were denatured with SDS sample buffer and heated for 10 min at 95°C. Following separation by SDS-PAGE at 80 to 120 V, proteins were blotted on a polyvinylidene difluoride (PVDF) membrane (Carl Roth, Karlsruhe, Germany). For total protein stain, membranes were stained directly after protein transfer using the Revert™ 700 Total Protein Stain kit (Li-cor Biosciences GmbH, Bad Homburg, Germany). Membranes were blocked with 10% milk in TBS-T or 1$\times$ RotiBlock (Carl Roth, Karlsruhe, Germany) and subsequently incubated with primary antibody, either overnight at 4°C with αTHN and αHRS (Santa Cruz Biotechnology, Dallas, USA), or 1 h at room temperature with αZIKV E (51) and αActin (Sigma-Aldrich, St. Louis, USA). Secondary antibody incubation was carried out with HRP- (GE Healthcare, Chicago, USA) or IRDye 680RD/IRDye 800CW-coupled antibodies (Li-cor Biosciences GmbH, Bad Homburg, Germany) 1 h at room temperature. Subsequently, signals were detected after the addition of peroxidase substrate reagent and either scientific imaging film exposure or using the ImageQuant™ 800 imaging system (Cytiva, Marlborough, USA). In the case of fluorophore-coupled secondary antibodies, the detection was carried out using the Licor-Odyssey imaging system (Li-cor Biosciences GmbH, Bad Homburg, Germany).

Indirect immunofluorescence microscopy. To carry out immunofluorescent staining, cells grown on coverslips were fixed for 20 min at room temperature with 3.7% formaldehyde (Carl Roth, Karlsruhe, Germany). Following membrane permeabilization for 10 min with 0.5% Triton X-100 (Sigma-Aldrich, St. Louis, USA), unspecific binding sites were blocked 15 min with 1% bovine serum albumin (BSA) fraction V (Carl Roth, Karlsruhe, Germany). Antibody incubations were carried out for 1 h at room temperature, respectively. As primary antibodies, αTHN (rabbit-derived, Proteintech, Rosemont, USA; mouse-derived, Santa Cruz Biotechnology, Dallas, USA), αflavivirus group antigen 4G2 (Merck Millipore, Darmstadt, Germany), αLAMP2 (BD Biosciences, NJ, USA) and αLC3 (MBL, Woburn, USA) were used. Alexa Fluor 488- (Thermo Fisher Scientific, Waltham, USA) or Cyanine Cy™3-conjugated antibodies (Jackson ImmunoResearch, West Grove, USA) served as secondary antibodies. Nuclei were stained with 4′,6-diamidino-2-phenylindole (DAPI, Carl Roth, Karlsruhe, Germany), while the actin cytoskeleton was visualized with phalloidin-Atto633 (Sigma-Aldrich, St. Louis, USA). After staining, slides were embedded with mowiol. Imaging was performed with the confocal laser scanning microscope Leica SP8 (Leica Camera AG, Wetzlar, Germany). Analysis was done using the LAS X (Leica Camera AG, Wetzlar, Germany) or FIJI software.

Polyinosinic:poly(C) (Poly I:C) treatment. After seeding of 6-well plates with a density of 3×10^5 cells per well, cells were treated with 4 μg/mL Poly I:C or left untreated. Sixteen hours after treatment, cells were either harvested or the treatment was renewed, and cells were harvested 8 h later for a subsequent Western blot.

Half-life determination. Determination of protein half-life was performed in uninfected cells or 16 to 18 h pi after infection with ZIKV Uganda at a MOI of 5. Cells were treated with 71 μM cycloheximide (CHX) to inhibit further protein translation and harvested at the indicated time points with RIPA buffer followed by SDS-PAGE and Western blot. The protein half-life was calculated from a nonlinear regression equation based on at least five independent experiments using the software GraphPad Prism (GraphPad Software, La Jolla, USA).

Treatment with inhibitors of protein degradation pathways. Uninfected cells or cells infected with ZIKV Uganda at a MOI of 5 were treated 16 h pi with inhibitors of different protein degradation pathways. Lysosomal acidification was inhibited with 50 nM Bafilomycin A1 (BFLA, Sigma-Aldrich, St. Louis, USA) (46), 50 mM NH_4Cl (Merck Millipore, Darmstadt, Germany) (52) or 50 μM Chloroquine (Sigma-Aldrich, St. Louis, USA) (53). Early steps of autophagy were inhibited using 20 μM LY294002 (Selleck Chemicals, Houston, USA), a PI3K-Inhibitor (54). Inhibition of proteasomal protein degradation was done with 1 μM Bortezomib (Selleck Chemicals, Houston, USA) (55) or 10 μM MG132 (Merck Millipore, Darmstadt, Germany) (56). Eight hours after treatment, cells were harvested and analyzed by Western blotting.

Knockdown of HRS with siRNA. Cells were transfected with 2 nM siRNA while seeding using the Lipofectamine™ RNAiMAX transfection reagent (Thermo Fisher, Waltham, USA) according to the manufacturer's instructions. HRS was targeted with the siRNA sequence CGACAAGAACCCACACGUCdTdT or UCCGCCAAGGGGACACACAAGdTdT (HRS siRNA 2) that have been previously described (34, 42, 57) and were purchased from Eurofins (Eurofins, Luxembourg, Luxembourg). Control siRNA-A (Santa Cruz Biotechnology, Dallas, USA) was used as scrambled control.

Binding assay. A ZIKV binding assay was performed as described before (58). In brief, cells were pre-chilled 30 min at 4°C and infected with ZIKV Polynesia or Uganda at a MOI of 0.1 for another 1 h at 4°C. Cells were washed once with PBS and harvested for quantification of bound ZIKV genomes by qPCR.

Statistical analysis. Results are described as mean ± standard deviation (SD) and are from at least three independent experiments unless stated otherwise. The significance of the results was analyzed by Student's *t* test performed on log-transformed data using the software GraphPad Prism (GraphPad Software, La Jolla, USA). Ns = not significant; * $P \leq 0.05$; ** $P \leq 0.01$; *** $P \leq 0.001$; **** $P \leq 0.0001$.

ACKNOWLEDGMENTS

We thank Gert Carra and Robin Murra for their exceptional technical support. We also thank Barbara Schnierle for providing the Vero eV, Vero-THN, HT-1080, and HT-1080-THN cell lines.

This research was funded by a grant from the LOEWE Center DRUID (Novel Drug Targets against Poverty-Related and Neglected Tropical Infectious Diseases) to D.B. and E.H. This publication was supported by the European Virus Archive goes Global (EVAg) project that has received funding from the European Union's Horizon 2020 research and innovation program under grant agreement No. 653316. Based on this funding, EVAg provided the ZIKV French Polynesia H/PF/2013 and the Uganda 976 strains.

We declare no conflict of interest.

REFERENCES

1. Musso D, Gubler DJ. 2016. Zika virus. Clin Microbiol Rev 29:487–524. https://doi.org/10.1128/CMR.00072-15.
2. World Health Organization. Zika virus. https://www.who.int/news-room/fact-sheets/detail/zika-virus. Accessed 29 September, 2021.
3. Sirohi D, Kuhn RJ. 2017. Zika virus structure, maturation, and receptors. J Infect Dis 216:S935–S944. https://doi.org/10.1093/infdis/jix515.
4. Sirohi D, Chen Z, Sun L, Klose T, Pierson TC, Rossmann MG, Kuhn RJ. 2016. The 3.8 Å resolution cryo-EM structure of Zika virus. Science 352:467–470. https://doi.org/10.1126/science.aaf5316.
5. Kostyuchenko VA, Lim EXY, Zhang S, Fibriansah G, Ng T-S, Ooi JSG, Shi J, Lok S-M. 2016. Structure of the thermally stable Zika virus. Nature 533:425–428. https://doi.org/10.1038/nature17994.
6. Pielnaa P, Al-Saadawe M, Saro A, Dama MF, Zhou M, Huang Y, Huang J, Xia Z. 2020. Zika virus-spread, epidemiology, genome, transmission cycle, clinical manifestation, associated challenges, vaccine and antiviral drug development. Virology 543:34–42. https://doi.org/10.1016/j.virol.2020.01.015.
7. Foy BD, Kobylinski KC, Chilson Foy JL, Blitvich BJ, Da Travassos Rosa A, Haddow AD, Lanciotti RS, Tesh RB. 2011. Probable non-vector-borne transmission of Zika virus, Colorado, USA. Emerg Infect Dis 17:880–882. https://doi.org/10.3201/eid1705.101939.
8. Magnus MM, Espósito DLA, Da Costa VA, de Melo PS, Costa-Lima C, Da Fonseca BAL, Addas-Carvalho M. 2018. Risk of Zika virus transmission by blood donations in Brazil. Hematol Transfus Cell Ther 40:250–254. https://doi.org/10.1016/j.htct.2018.01.011.
9. Barjas-Castro ML, Angerami RN, Cunha MS, Suzuki A, Nogueira JS, Rocco IM, Maeda AY, Vasami FGS, Katz G, Boin IFSF, Stucchi RSB, Resende MR, Esposito DLA, de Souza RP, Da Fonseca BA, Addas-Carvalho M. 2016. Probable transfusion-transmitted Zika virus in Brazil. Transfusion 56:1684–1688. https://doi.org/10.1111/trf.13681.
10. Besnard M, Lastère S, Teissier A, Cao-Lormeau VM, Musso D. 2014. Evidence of perinatal transmission of Zika virus, French Polynesia, December 2013 and February 2014. Eurosurveillance 19:20751. https://doi.org/10.2807/1560-7917.ES2014.19.13.20751.
11. Hamel R, Dejarnac O, Wichit S, Ekchariyawat P, Neyret A, Luplertlop N, Perera-Lecoin M, Surasombatpattana P, Talignani L, Thomas F, Cao-Lormeau V-M, Choumet V, Briant L, Desprès P, Amara A, Yssel H, Missé D. 2015. Biology of Zika Virus Infection in Human Skin Cells. J Virol 89:8880–8896. https://doi.org/10.1128/JVI.00354-15.
12. Sabino C, Bender D, Herrlein M-L, Hildt E. 2021. The Epidermal Growth Factor Receptor Is a Relevant Host Factor in the Early Stages of The Zika Virus Life Cycle In Vitro. J Virol 95:e0119521. https://doi.org/10.1128/JVI.01195-21.
13. Sager G, Gabaglio S, Sztul E, Belov GA. 2018. Role of Host Cell Secretory Machinery in Zika Virus Life Cycle. Viruses 10:559. https://doi.org/10.3390/v10100559.
14. Cortese M, Goellner S, Acosta EG, Neufeldt CJ, Oleksiuk O, Lampe M, Haselmann U, Funaya C, Schieber N, Ronchi P, Schorb M, Pruunsild P, Schwab Y, Chatel-Chaix L, Ruggieri A, Bartenschlager R. 2017. Ultrastructural Characterization of Zika Virus Replication Factories. Cell Rep 18:2113–2123. https://doi.org/10.1016/j.celrep.2017.02.014.
15. Yu I-M, Zhang W, Holdaway HA, Li L, Kostyuchenko VA, Chipman PR, Kuhn RJ, Rossmann MG, Chen J. 2008. Structure of the immature dengue virus at low pH primes proteolytic maturation. Science 319:1834–1837. https://doi.org/10.1126/science.1153264.
16. Owczarek K, Chykunova Y, Jassoy C, Maksym B, Rajfur Z, Pyrc K. 2019. Zika virus: mapping and reprogramming the entry. Cell Commun Signal 17:41. https://doi.org/10.1186/s12964-019-0349-z.
17. Liu J, Kline BA, Kenny TA, Smith DR, Soloveva V, Beitzel B, Pang S, Lockett S, Hess HF, Palacios G, Kuhn JH, Sun MG, Zeng X. 2018. A novel sheet-like virus particle array is a hallmark of Zika virus infection. Emerg Microbes Infect 7:69. https://doi.org/10.1038/s41426-018-0071-8.
18. Burlaud-Gaillard J, Sellin C, Georgeault S, Uzbekov R, Lebos C, Guillaume J-M, Roingeard P. 2014. Correlative scanning-transmission electron microscopy reveals that a chimeric flavivirus is released as individual particles in secretory vesicles. PLoS One 9:e93573. https://doi.org/10.1371/journal.pone.0093573.
19. Le Tortorec A, Willey S, Neil SJD. 2011. Antiviral inhibition of enveloped virus release by tetherin/BST-2: action and counteraction. Viruses 3:520–540. https://doi.org/10.3390/v3050520.
20. Neil SJD, Zang T, Bieniasz PD. 2008. Tetherin inhibits retrovirus release and is antagonized by HIV-1 Vpu. Nature 451:425–430. https://doi.org/10.1038/nature06553.
21. Kaletsky RL, Francica JR, Agrawal-Gamse C, Bates P. 2009. Tetherin-mediated restriction of filovirus budding is antagonized by the Ebola glycoprotein. Proc Natl Acad Sci U S A 106:2886–2891. https://doi.org/10.1073/pnas.0811014106.
22. Sakuma T, Noda T, Urata S, Kawaoka Y, Yasuda J. 2009. Inhibition of Lassa and Marburg virus production by tetherin. J Virol 83:2382–2385. https://doi.org/10.1128/JVI.01607-08.
23. Mansouri M, Viswanathan K, Douglas JL, Hines J, Gustin J, Moses AV, Früh K. 2009. Molecular mechanism of BST2/tetherin downregulation by K5/MIR2 of Kaposi's sarcoma-associated herpesvirus. J Virol 83:9672–9681. https://doi.org/10.1128/JVI.00597-09.
24. Pan X-B, Han J-C, Cong X, Wei L. 2012. BST2/tetherin inhibits dengue virus release from human hepatoma cells. PLoS One 7:e51033. https://doi.org/10.1371/journal.pone.0051033.
25. Li M, Wang P, Zheng Z, Hu K, Zhang M, Guan X, Fu M, Zhang D, Wang W, Xiao G, Hu Q, Liu Y. 2017. Japanese encephalitis virus counteracts BST2 restriction via its envelope protein E. Virology 510:67–75. https://doi.org/10.1016/j.virol.2017.07.008.

26. Venkatesh S, Bieniasz PD. 2013. Mechanism of HIV-1 virion entrapment by tetherin. PLoS Pathog 9:e1003483. https://doi.org/10.1371/journal.ppat.1003483.
27. Truebestein L, Leonard TA. 2016. Coiled-coils: the long and short of it. Bioessays 38:903–916. https://doi.org/10.1002/bies.201600062.
28. Edgar JR, Manna PT, Nishimura S, Banting G, Robinson MS. 2016. Tetherin is an exosomal tether. Elife 5:e17180. https://doi.org/10.7554/eLife.17180.
29. Sharma A, Lal SK. 2019. Is tetherin a true antiviral: the influenza a virus controversy. Rev Med Virol 29:e2036. https://doi.org/10.1002/rmv.2036.
30. Schmidt S, Fritz JV, Bitzegeio J, Fackler OT, Keppler OT. 2011. HIV-1 Vpu blocks recycling and biosynthetic transport of the intrinsic immunity factor CD317/tetherin to overcome the virion release restriction. mBio 2:e00036-11–e00011. https://doi.org/10.1128/mBio.00036-11.
31. Pardieu C, Vigan R, Wilson SJ, Calvi A, Zang T, Bieniasz P, Kellam P, Towers GJ, Neil SJD. 2010. The RING-CH ligase K5 antagonizes restriction of KSHV and HIV-1 particle release by mediating ubiquitin-dependent endosomal degradation of tetherin. PLoS Pathog 6:e1000843. https://doi.org/10.1371/journal.ppat.1000843.
32. Lopez LA, Yang SJ, Hauser H, Exline CM, Haworth KG, Oldenburg J, Cannon PM. 2010. Ebola virus glycoprotein counteracts BST-2/Tetherin restriction in a sequence-independent manner that does not require tetherin surface removal. J Virol 84:7243–7255. https://doi.org/10.1128/JVI.02636-09.
33. Paliwal D, Joshi P, Panda SK. 2017. Hepatitis E Virus (HEV) egress: role of BST2 (Tetherin) and interferon induced long non- coding RNA (lncRNA) BISPR. PLoS One 12:e0187334. https://doi.org/10.1371/journal.pone.0187334.
34. Janvier K, Pelchen-Matthews A, Renaud J-B, Caillet M, Marsh M, Berlioz-Torrent C. 2011. The ESCRT-0 component HRS is required for HIV-1 Vpu-mediated BST-2/tetherin down-regulation. PLoS Pathog 7:e1001265. https://doi.org/10.1371/journal.ppat.1001265.
35. Toyoshima M, Tanaka N, Aoki J, Tanaka Y, Murata K, Kyuuma M, Kobayashi H, Ishii N, Yaegashi N, Sugamura K. 2007. Inhibition of tumor growth and metastasis by depletion of vesicular sorting protein Hrs: its regulatory role on E-cadherin and beta-catenin. Cancer Res 67:5162–5171. https://doi.org/10.1158/0008-5472.CAN-06-2756.
36. Tabari D, Scholl C, Steffens M, Weickhardt S, Elgner F, Bender D, Herrlein M-L, Sabino C, Semkova V, Peitz M, Till A, Brüstle O, Hildt E, Stingl J. 2020. Impact of Zika Virus Infection on Human Neural Stem Cell MicroRNA Signatures. Viruses 12:1219. https://doi.org/10.3390/v12111219.
37. Gratton R, Agrelli A, Tricarico PM, Brandão L, Crovella S. 2019. Autophagy in Zika Virus Infection: a Possible Therapeutic Target to Counteract Viral Replication. Int J Mol Sci 20:1048. https://doi.org/10.3390/ijms20051048.
38. Liang Q, Luo Z, Zeng J, Chen W, Foo S-S, Lee S-A, Ge J, Wang S, Goldman SA, Zlokovic BV, Zhao Z, Jung JU. 2016. Zika Virus NS4A and NS4B Proteins Deregulate Akt-mTOR Signaling in Human Fetal Neural Stem Cells to Inhibit Neurogenesis and Induce Autophagy. Cell Stem Cell 19:663–671. https://doi.org/10.1016/j.stem.2016.07.019.
39. Raiborg C, Stenmark H. 2009. The ESCRT machinery in endosomal sorting of ubiquitylated membrane proteins. Nature 458:445–452. https://doi.org/10.1038/nature07961.
40. Puertollano R, Bonifacino JS. 2004. Interactions of GGA3 with the ubiquitin sorting machinery. Nat Cell Biol 6:244–251. https://doi.org/10.1038/ncb1106.
41. Puertollano R. 2005. Interactions of TOM1L1 with the multivesicular body sorting machinery. J Biol Chem 280:9258–9264. https://doi.org/10.1074/jbc.M412481200.
42. Bache KG, Brech A, Mehlum A, Stenmark H. 2003. Hrs regulates multivesicular body formation via ESCRT recruitment to endosomes. J Cell Biol 162:435–442. https://doi.org/10.1083/jcb.200302131.
43. Bieniasz PD. 2009. The cell biology of HIV-1 virion genesis. Cell Host Microbe 5:550–558. https://doi.org/10.1016/j.chom.2009.05.015.
44. Watanabe T, Sorensen EM, Naito A, Schott M, Kim S, Ahlquist P. 2007. Involvement of host cellular multivesicular body functions in hepatitis B virus budding. Proc Natl Acad Sci U S A 104:10205–10210. https://doi.org/10.1073/pnas.0704000104.
45. Elgner F, Ren H, Medvedev R, Ploen D, Himmelsbach K, Boller K, Hildt E. 2016. The Intracellular Cholesterol Transport Inhibitor U18666A Inhibits the Exosome-Dependent Release of Mature Hepatitis C Virus. J Virol 90:11181–11196. https://doi.org/10.1128/JVI.01053-16.
46. Sabino C, Basic M, Bender D, Elgner F, Himmelsbach K, Hildt E. 2019. Bafilomycin A1 and U18666A Efficiently Impair ZIKV Infection. Viruses 11:524. https://doi.org/10.3390/v11060524.
47. Yan R, Zhao X, Cai D, Liu Y, Block TM, Guo J-T, Guo H. 2015. The Interferon-Inducible Protein Tetherin Inhibits Hepatitis B Virus Virion Secretion. J Virol 89:9200–9212. https://doi.org/10.1128/JVI.00933-15.
48. Maddaluno L, Urwyler C, Rauschendorfer T, Meyer M, Stefanova D, Spörri R, Wietecha M, Ferrarese L, Stoycheva D, Bender D, Li N, Strittmatter G, Nasirujjaman K, Beer H-D, Staeheli P, Hildt E, Oxenius A, Werner S. 2020. Antagonism of interferon signaling by fibroblast growth factors promotes viral replication. EMBO Mol Med 12:e11793. https://doi.org/10.15252/emmm.201911793.
49. Schemmerer M, Apelt S, Trojnar E, Ulrich RG, Wenzel JJ, Johne R. 2016. Enhanced Replication of Hepatitis E Virus Strain 47832c in an A549-Derived Subclonal Cell Line. Viruses 8:267. https://doi.org/10.3390/v8100267.
50. Glitscher M, Himmelsbach K, Woytinek K, Schollmeier A, Johne R, Praefcke GJK, Hildt E. 2021. Identification of the interferon-inducible GTPase GBP1 as major restriction factor for the Hepatitis E virus. J Virol 95:e01564-20. https://doi.org/10.1128/JVI.01564-20.
51. Akhras S, Herrlein M-L, Elgner F, Holzhauser T, Hildt E. 2019. ZIKV Envelope Domain-Specific Antibodies: production, Purification and Characterization. Viruses 11:748. https://doi.org/10.3390/v11080748.
52. Wang H, Yuan X, Sun Y, Mao X, Meng C, Tan L, Song C, Qiu X, Ding C, Liao Y. 2019. Infectious bronchitis virus entry mainly depends on clathrin mediated endocytosis and requires classical endosomal/lysosomal system. Virology 528:118–136. https://doi.org/10.1016/j.virol.2018.12.012.
53. Fedele AO, Proud CG. 2020. Chloroquine and bafilomycin A mimic lysosomal storage disorders and impair mTORC1 signalling. Biosci Rep 40:BSR2020090. https://doi.org/10.1042/BSR20200905.
54. Johnson RA, Wang X, Ma XL, Huong SM, Huang ES. 2001. Human cytomegalovirus up-regulates the phosphatidylinositol 3-kinase (PI3-K) pathway: inhibition of PI3-K activity inhibits viral replication and virus-induced signaling. J Virol 75:6022–6032. https://doi.org/10.1128/JVI.75.13.6022-6032.2001.
55. Fournier M-J, Gareau C, Mazroui R. 2010. The chemotherapeutic agent bortezomib induces the formation of stress granules. Cancer Cell Int 10:12. https://doi.org/10.1186/1475-2867-10-12.
56. Llamas-González YY, Campos D, Pascale JM, Arbiza J, González-Santamaría J. 2019. A Functional Ubiquitin-Proteasome System is Required for Efficient Replication of New World Mayaro and Una Alphaviruses. Viruses 11:370. https://doi.org/10.3390/v11040370.
57. Vieira OV, Harrison RE, Scott CC, Stenmark H, Alexander D, Liu J, Gruenberg J, Schreiber AD, Grinstein S. 2004. Acquisition of Hrs, an essential component of phagosomal maturation, is impaired by mycobacteria. Mol Cell Biol 24:4593–4604. https://doi.org/10.1128/MCB.24.10.4593-4604.2004.
58. Basic M, Elgner F, Bender D, Sabino C, Herrlein M-L, Roth H, Glitscher M, Fath A, Kerl T, Schmalz H-G, Hildt E. 2019. A synthetic derivative of houttuynoid B prevents cell entry of Zika virus. Antiviral Res 172:104644. https://doi.org/10.1016/j.antiviral.2019.104644.